Romanian Reports in Physics, Vol. 63, No. 2, P. 383–393, 2011

PRIMARY ENERGY RECONSTRUCTION FROM THE S(500) OBSERVABLE RECORDED WITH THE KASCADE-GRANDE DETECTOR ARRAY*

G. TOMA[4], W.D. APEL[1], J.C. ARTEAGA[2,10], F. BADEA[1], K. BEKK[1], M. BERTAINA[3], J. BLÜMER[1,2], H. BOZDOG[1], I.M. BRANCUS[4], M. BRÜGGEMANN[5], P. BUCHHOLZ[5], E. CANTONI[3,6], A. CHIAVASSA[3], F. COSSAVELLA[2], K. DAUMILLER[1], V. DE SOUZA[2,11], F. DI PIERRO[3], P. DOLL[1], R. ENGEL[1], J. ENGLER[1], M. FINGER[1], D. FUHRMANN[7], P.L. GHIA[6], H.J. GILS[1], R. GLASSTETTER[7], C. GRUPEN[5], A. HAUNGS[1], D. HECK[1], J.R. HÖRANDEL[2,12], T. HUEGE[1], P.G. ISAR[1], K.-H. KAMPERT[7], D. KANG[2], D. KICKELBICK[5], H.O. KLAGES[1], P. ŁUCZAK[8], H.J. MATHES[1], H.J. MAYER[1], J. MILKE[1], B. MITRICA[4], C. MORELLO[6], G. NAVARRA[3], S. NEHLS[1], J. OEHLSCHLÄGER[1], S. OSTAPCHENKO[1,13], S. OVER[5], M. PETCU[4], T. PIEROG[1], H. REBEL[1], M. ROTH[1], H. SCHIELER[1], F. SCHRÖDER[1], O. SIMA[9], M. STÜMPERT[2], G.C. TRINCHERO[6], H. ULRICH[1], A. WEINDL[1], J. WOCHELE[1], M. WOMMER[1], J. ZABIEROWSKI[8]

[1]Institut für Kernphysik, Forschungszentrum Karlsruhe, 76021 Karlsruhe, Germany
[2]Institut für Experimentelle Kernphysik, Universität Karlsruhe, 76021 Karlsruhe, Germany
[3]Dipartimento di Fisica Generale dell'Università, 10125 Torino, Italy
[4]"Horia Hulubei"National Institute of Physics and Nuclear Engineering, 077125 Bucharest, Măgurele Romania
[5]Fachbereich Physik, Universität Siegen, 57068 Siegen, Germany
[6]Istituto di Fisica dello Spazio Interplanetario, INAF, 10133 Torino, Italy
[7]Fachbereich Physik, Universität Wuppertal, 42097 Wuppertal, Germany
[8]Soltan Institute for Nuclear Studies, 90950 Lodz, Poland
[9]Department of Physics, University of Bucharest, 76900 Bucharest, Romania
[10]now at: Universidad Michoacana, Morelia, Mexico
[11]now at: Universidade de São Paulo, Instituto de Fîsica de São Carlos, Brasil
[12]now at: Dept. of Astrophysics, Radboud University Nijmegen, The Netherlands
[13]now at: University of Trondheim, Norway
toma@ik.fzk.de

Received January 20, 2010

Abstract. Previous EAS investigations have shown that the charged particle density becomes independent of the primary mass at large but fixed distances from the shower core and that it can be used as an estimator for the primary energy. The particular radial distance from the shower axis where this effect takes place is dependent on the detector layout. For the KASCADE-Grande experiment,

* Paper presented at the Annual Scientific Session of Faculty of Physics, University of Bucharest, June 5, 2009, Bucharest – Măgurele, Romania.

simulation studies have shown it to be around 500 m. A notation $S(500)$ is used for the charged particle density at this specific distance. We present results on the reconstruction of the primary energy spectrum of cosmic rays from the experimentally recorded $S(500)$ observable using the KASCADE-Grande array. The constant intensity cut (CIC) method is applied to evaluate the attenuation of the $S(500)$ observable with the zenith angle. A correction is subsequently applied to correct all recorded $S(500)$ values for attenuation. The all event $S(500)$ spectrum is obtained. A calibration of $S(500)$ values with the primary energy has been worked out by simulations and has been used for conversion thus obtaining the primary energy spectrum (in the energy range accessible to the KASCADE-Grande array of 10^{16}-10^{18} eV). An evaluation of systematic uncertainties induced by different sources is also given.

Key words: KASCADE-Grande, EAS, primary energy spectrum.

1. INTRODUCTION

Hillas has shown that the EAS particle density distributions at a certain distance from the shower core (dependent on the EAS detection array) becomes independent of the primary mass and can be used as a primary energy estimator [1]. Following this feature, a method can be derived to reconstruct the primary energy spectrum from the particular value of the charged particle density, observed at such specific radial ranges. The technique has been used by different detector arrays in order to reconstruct the primary energy spectrum of the cosmic radiation [2]. In the case of the KASCADE-Grande array (at Forschungszentrum Karlsruhe, Germany, 110 m a.s.l.) [3], detailed simulations [4] have shown that the particular distance for which this effect takes place is about 500 m (see Fig. 1). Therefore an observable of interest in the case of KASCADE-Grande is the charged particle density at 500 m distance from the shower core, noted as $S(500)$ in the following. The study has been performed for both simulated (Fig. 1) and experimental (Fig. 2) events, using identical reconstruction procedures [5]. The reconstruction begins with recording the energy deposits of particles in the KASCADE-Grande detector stations and the associated temporal information (arrival times of particles). The arrival direction of the shower is reconstructed from the particle arrival times. Using appropriate **L**ateral **E**nergy **C**orrection **F**unctions (**LECF**), the energy deposits are converted into particle densities. The LECF functions take into account the fact that an inclined particle will deposit more energy in detectors due to its longer cross path [6]. Unlike in the case of simulated events where the particle density is accesible at any radial range, the experimental event is described only by the data recorded in each detector station, therefore the experimentally measured lateral particle density will be a distribution of (at best) up to 37 points (considering the number of detector stations in the Grande detector array). In order to obtain the particle density of interest at 500 m distance from shower core, a

parameterisation must be applied to describe the lateral particle density distribution. A Linsley **L**ateral **D**ensity **F**unction (**LDF**) (eq. 1, [7]) is used for this purpose. To ensure good reconstruction quality, the approximation is performed over a limited range of the lateral extension, namely only in the 40 m – 1000 m radial range.

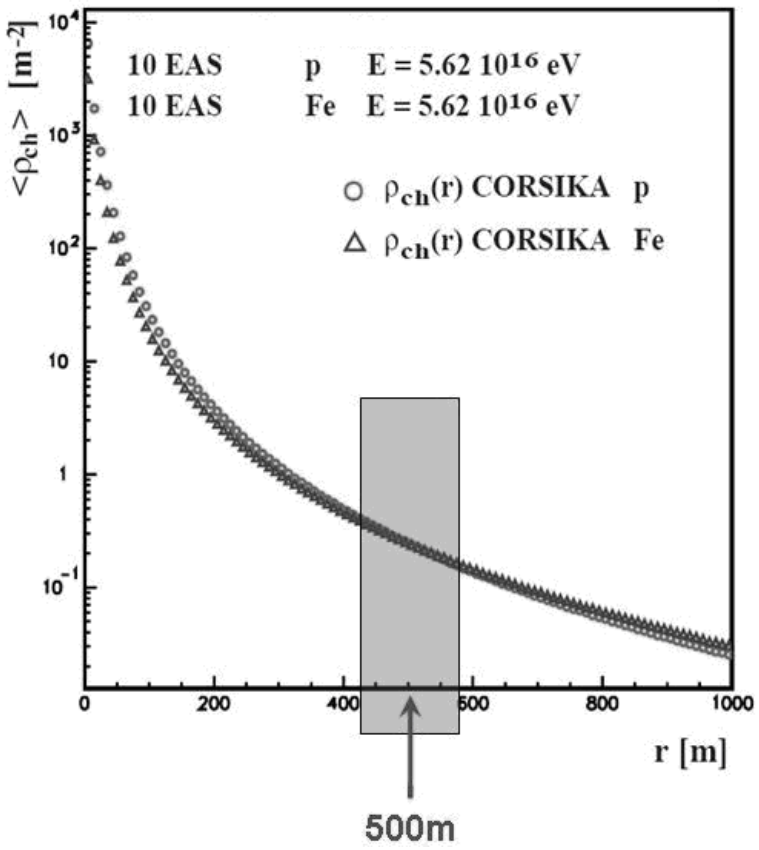

Fig. 1 – Simulations show that, for the case of the KASCADE-Grande experimental layout, the particle density becomes independent of the primary mass around 500m distance from shower core; this plot shows averaged simulated lateral distributions for different primary types with equal energy.

$$\rho(r), S(r) = \frac{N}{2\pi \cdot r_0^2} \cdot \frac{\Gamma(\eta - \alpha)}{\Gamma(2-\alpha)\cdot\Gamma(\eta-2)} \left(\frac{r}{r_0}\right)^{-\alpha} \left(1+\frac{r}{r_0}\right)^{-(\eta-\alpha)}, \quad (1)$$

where: $\rho(r)$, $S(r)$ – real/reconstructed particle density at distance r [m] from shower core; N – "shower size" (in this case the total number of charged particles); r_0 – Molière radius [meters]; r – radius [meters]; α, η – slope parameters (previous studies have shown a limited mass sensitivity for the η parameter).

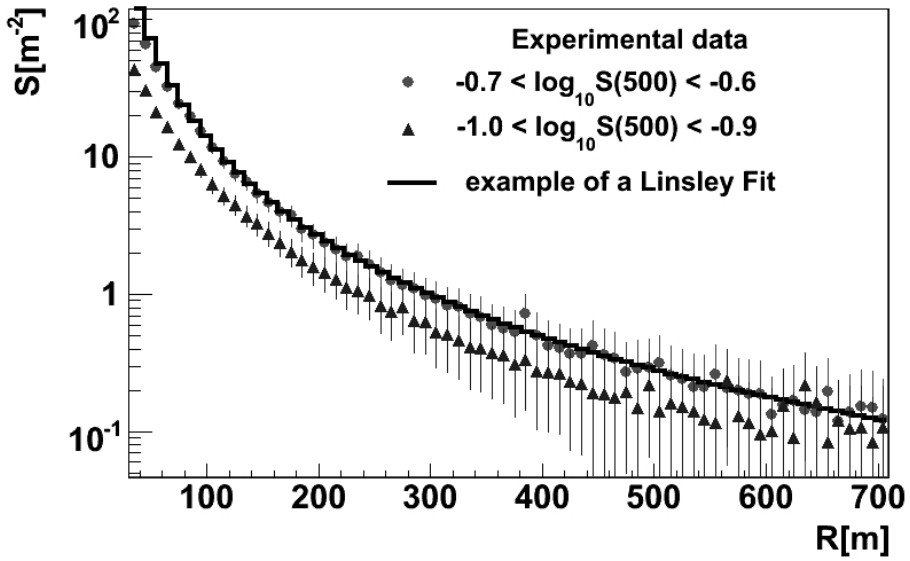

Fig. 2 – Averaged lateral density distributions of experimentally recorded EAS samples for two $S(500)$ ranges.

2. THE KASCADE-GRANDE ARRAY

The extensive air showers can be detected by a number of detector arrangements, a widely spread solution being the detector array. Such an array is the KASCADE-Grande array, situated at Forschungszentrum Karlsruhe, Germany (110 m a.s.l.) (Fig. 3). The array has a roughly quadratic shape with a length of ≈ 700 m and it is a complex detector system made of various types of detectors capable of registering different EAS observables. Historically, the KASCADE-Grande detector array began as a smaller array (the KASCADE array). KASCADE was designed to record air showers initiated by primaries with energies in the 10^{14}–10^{16} eV range (including the knee range). Later, when wanting to extend the energy range of detectable primaries (to 10^{16}–10^{18} eV), the Grande array was added to the already operating KASCADE array and thus the new KASCADE-Grande array began its operation. The reason for extending the size of the array was twofold. On one hand, higher energy showers come with lower intensity and thus, in order to record a reasonable amount of events in a reasonable amount of time, a larger array would be necessary.

The other aspect comes from the functionality of detectors themselves. High energy primaries generate high energy particle rich showers that tend to overflow detector stations close to shower core (where the particle density is very high). Thus, for a small array, data recorded close to shower core is not reliable and it is

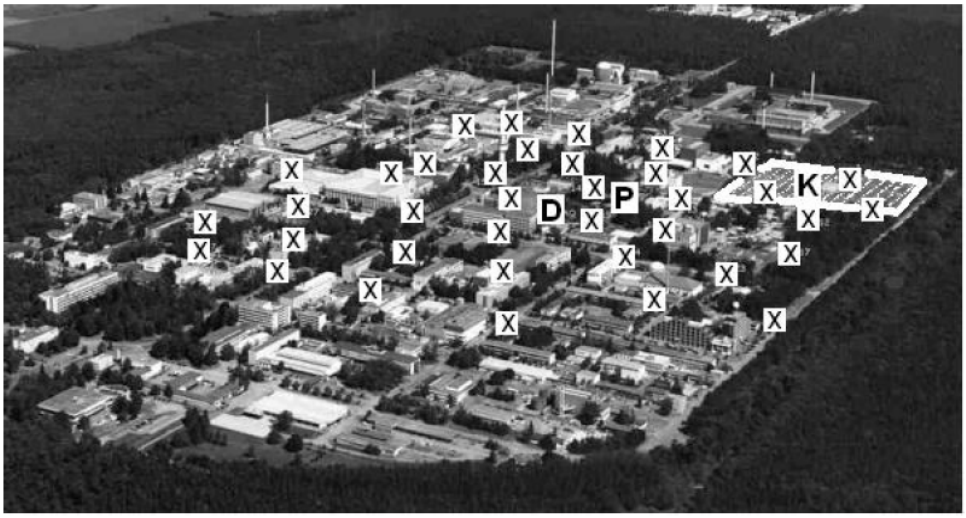

Fig. 3 – The KASCADE-Grande detector array with its components: the KASCADE array (K – the upper right rectangular area), the Digital Acquisition Station (D), the Grande stations (X), the Piccollo trigger array (P).

necessary to extract data from the EAS front at greater radial distances. The Grande array consists of 37 huts with 10 m^2 sensitive scintillator detector area, each. As opposed to the original KASACADE stations, the Grande stations do not have the ability to disentangle the type of particle hitting them. A technique was therefore developed to reconstruct the density of particles in detectors from the registered energy deposits.

3. EFFICIENCY AND QUALITY CUTS

For the experimental EAS sample, the total time of acquisition was ≈ 902 days. Showers were detected on a 500 × 600 m^2 fiducial area up to 30^o zenith angle. The 30^o zenith angle limit was imposed due to certain systematic effects affecting the reconstruction of small showers above this threshold. In order to ensure good reconstruction quality, several quality cuts were imposed on the data. The same cuts were used for both simulated and experimental events. Only those events are accepted for which the reconstructed shower core is positioned inside the detector array and not too close to the border. A good quality of the fit to the Linsley distribution is a further important criterion. Fig. 4 shows the total reconstruction efficiency for different zenith angle intervals (the full efficiency is reached at around $\log_{10}(E_0/\mathrm{GeV})=7.5$).

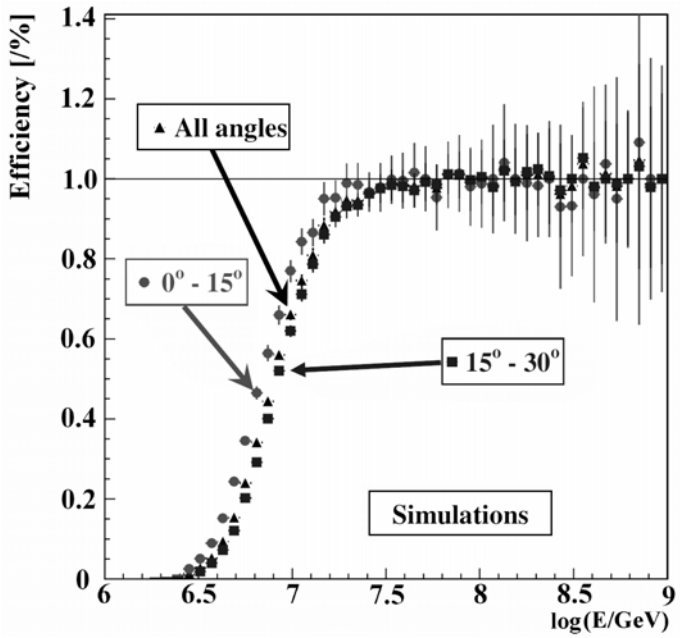

Fig. 4 – Reconstruction efficiency for different zenith angle ranges and for the entire shower sample (events triggering more than 24 stations); values greater than 1 for the total efficiency are due to EAS events that have the true core outside the fiducial area, but are reconstructed inside the fiducial area.

4. THE CONSTANT INTENSITY CUT METHOD

Prior to converting the recorded $S(500)$ values into the corresponding primary energy values (via a relation derived from simulation studies), one has to take into account the atmospheric attenuation affecting the charged particle densities observed on ground. For more inclined showers, the particles have to cross a longer path through the atmosphere before reaching the detector level. In such a case, events generated by identical primaries reach the detector level at different stages of EAS development, dependent on their angles of incidence. In order to bring all recorded EAS events to the same level of consistency, one has to remove the influence of the zenith angle on the recorded $S(500)$ observables. This is achieved by applying the **C**onstant **I**ntensity **C**ut (**CIC**) method. The $S(500)$ attenuation is visible if $S(500)$ spectra are plotted for different EAS incident angles. For this, the recorded events are separated into several sub-samples characterized by their angle of incidence. The angular intervals are chosen in a way that they open equal solid angles: 0^o – 13.2^o, 13.2^o – 18.8^o, 18.8^o – 23.1^o, 23.1^o – 26.7^o and 26.7^o – 30.0^o. In Fig. 4 the attenuation is visible, as $S(500)$ spectra are shifted towards lower values for increasing zenith angles.

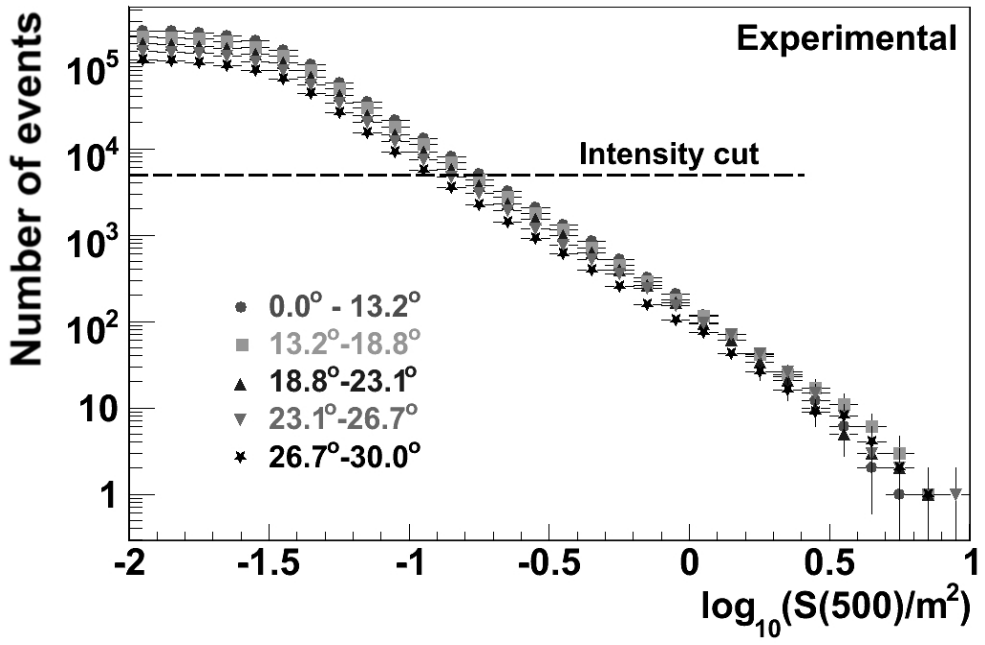

Fig. 5 – Integral *S*(500) spectra; the horizontal line is a constant intensity cut at an arbitrarily chosen intensity.

The CIC method assumes that a given intensity value in the energy spectrum corresponds to a given primary energy of particles and, since the *S*(500) is mapping the primary energy spectrum, it is expected that this property of the intensity is true also in the case of *S*(500) spectra. Therefore a constant intensity cut on integral *S*(500) spectra is performed, effectively cutting them at a given primary energy. The intersection of the cut line with each spectrum will give the attenuated *S*(500) value at the corresponding angle of incidence for a given primary energy. A linear interpolation is used between the two neighboring points in the integral spectrum in order to convert the value of the intensity into particle density for each angular bin. The observed attenuation can be corrected by parameterizing the attenuation curve and correcting all events by bringing their *S*(500) value to their corresponding value at a given reference angle of incidence (see Fig. 6; the parameterization with the lowest χ^2 was chosen, namely the one corresponding to intensity 3 000). For the present study this angle is considered to be 21°, since the zenith angular distribution for the recorded EAS sample peaks at this value. The CIC method implies several mathematical transformations of data before obtaining the values corrected for attenuation of the *S*(500) observable: interpolations and analytical parameterizations (as mentioned in the above description of the CIC method).

These operations introduce some systematic uncertainties on the final result of the CIC method. The CIC-induced systematic uncertainty of the corrected

S(500) value is evaluated by propagating the errors of fit parameters. The resulting CIC-induced error of the *S*(500) observable will be taken into account later when evaluating the total systematic uncertainty of the reconstructed primary energy.

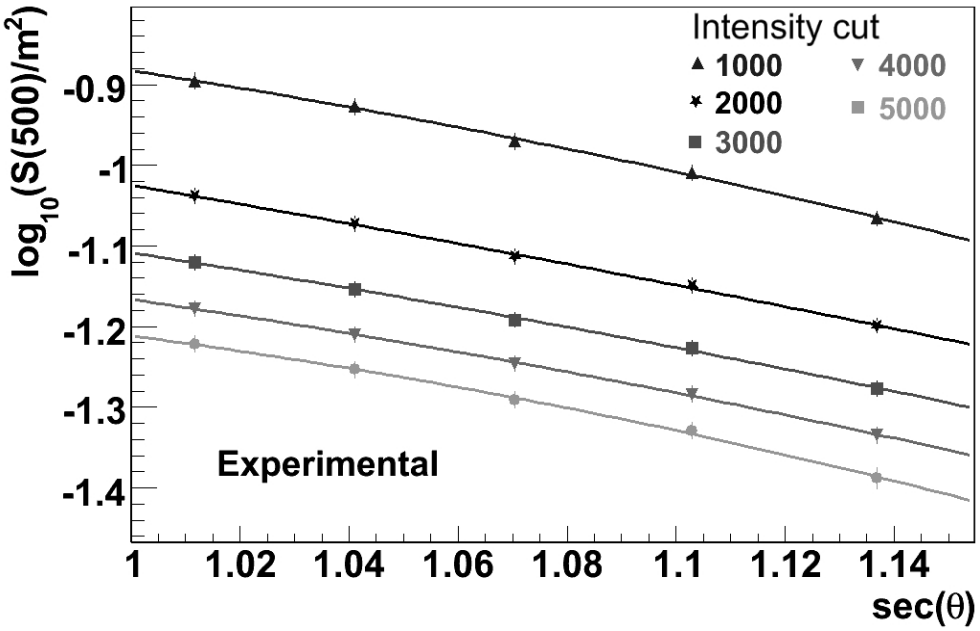

Fig. 6 – Attenuation of the *S*(500) observable with the angle of incidence; the different curves show different arbitrarily chosen intensity cuts; attenuation length of *S*(500) was evaluated to 754 ± 27 g·cm^{-2}.

5. CONVERSION TO ENERGY

After correcting each recorded *S*(500) value for attenuation, we can convert it to the corresponding primary energy value. A calibration of the primary energy E_0 with *S*(500) was derived from simulations (see Fig. 7). The Monte-Carlo CORSIKA EAS simulation tool was used to simulate air showers (with QGSJET II model embedded for high energy interactions). In Fig. 7, two nearly identical dependencies are shown for two primaries, a light primary (proton) and a heavy primary (Fe). The similarity of the two calibration curves derives from the mass insensitivity of the *S*(500).

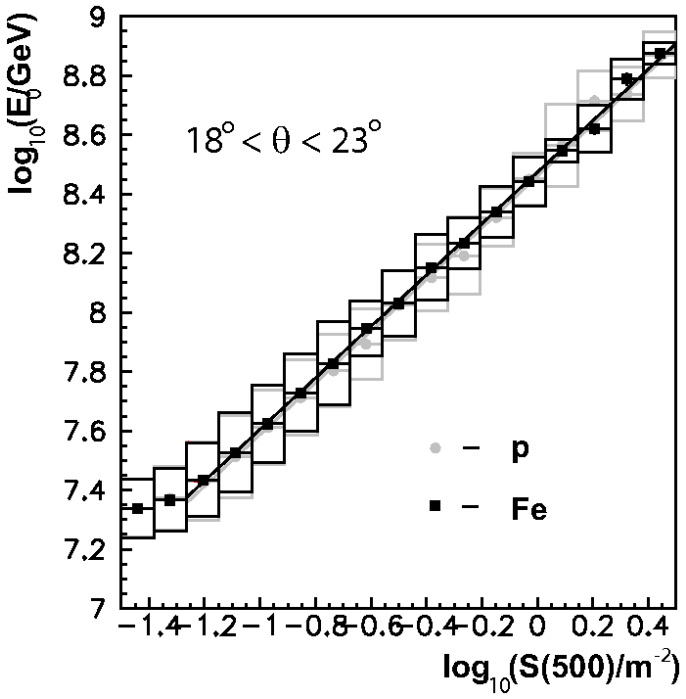

Fig. 7 – E_0 - $S(500)$ calibration curve for two different primaries; the box-errors are the errors on the spread; the errors on the mean are represented with bars.

This calibration is used to convert all $S(500)$ values into the corresponding primary energies. The spectrum of primary energy is thus reconstructed. Fig. 8 shows the reconstructed energy spectrum compared with spectra reconstructed by other experiments.

The spectrum is plotted starting from the maximum efficiency threshold (see Fig. 4). For the systematic contribution to the total error, several sources of systematic uncertainties have been identified and their contributions were evaluated. Thus, the spectral index of the simulated shower sample was equal to –2 and was acting as a source of systematic uncertainty. In a similar fashion, the E_0- $S(500)$ calibration and the CIC method itself were also introducing systematic uncertainties. In all, these three sources were contributing with an uncertainty of ≈1% from the total flux value. Other sources that were considered were the Monte-Carlo statistical uncertainty of the simulated shower sample and the choosing of a certain reference angle at which to perform the $S(500)$ attenuation correction (contributing with ≈7% and ≈30% relative uncertainty, respectively). The relative contribution of all identified sources over the full efficiency range was fairly constant for any given source and in total amounts for about 37% of the recorded flux value. The energy resolution has also been evaluated from simulations by

calculating the difference between the true and the reconstructed primary energy (applying CIC to the simulated data). The energy resolution was found to be 22% for $E_0=10^{17}$ eV (for all primaries) and is fairly constant over the entire full efficiency range.

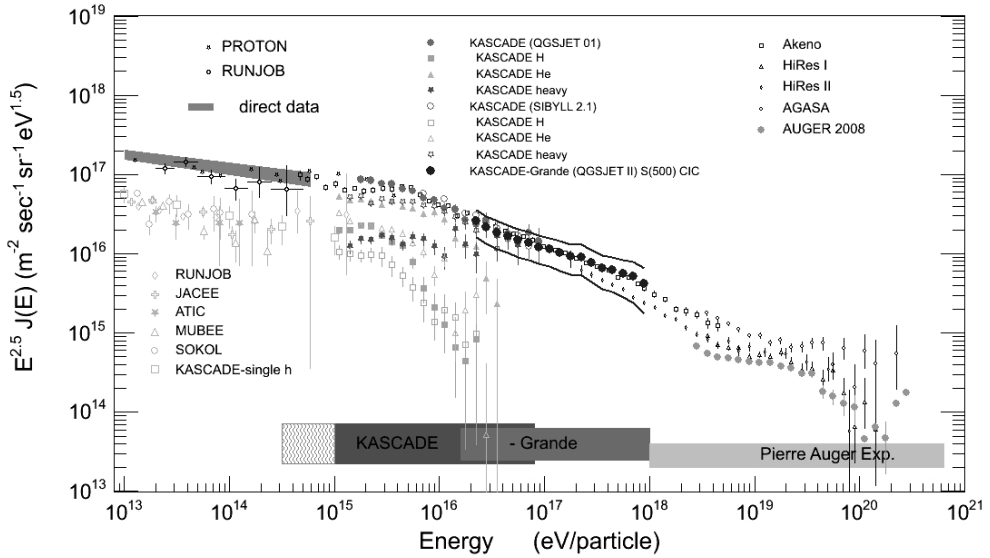

Fig. 8 – Reconstructed experimental energy spectrum by KASCADE-Grande from $S(500)$/CIC, multiplied by $E^{2.5}$ compared with results of other experiments; the continuous lines above and below the spectrum are the error envelopes and show combined statistical and systematic uncertainties.

6. CONCLUSIONS

The primary energy spectrum has been reconstructed from the particle densities recorded in the stations of the KASCADE-Grande array. In the particular case of KASCADE-Grande, the charged particle density at 500 m distance from the shower core was shown to be primary mass insensitive. The CIC method was applied on the recorded $S(500)$ spectrum in order to correct each shower for attenuation effects. Using a simulation-derived calibration between $S(500)$ and E_0 (based on the QGSJET II model for high energy interactions), the attenuation corrected $S(500)$ spectrum has been converted into primary energy spectrum. The $S(500)$ derived KASCADE-Grande spectrum is composition independent and is in good agreement with the spectrum of lower energies previously reconstructed by the KASCADE array. Future investigations will concentrate also on improving the quality of the reconstruction along with gaining a better understanding of the uncertainties induced by the reconstruction technique.

Acknowledgments. The KASCADE-Grande experiment is supported by the BMBF of Germany, the MIUR and INAF of Italy, the Polish Ministry of Science and Higher Education (Grant 2009-2011), and the Romanian Autority for Scientific Research, UEFISCDI, grant PNII-IDEI no. 461/2009 and grant PN 09370105. Part of the investigation was funded in the frame of the DAAD doctoral scholarship A/06/09016 Ref. 322 and by KIT Campus North in the frame of research visits.

REFERENCES

1. A. M. Hillas *et al.*, Proc.12th ICRC, Hobart, **3**, 1001 (1971).
2. D. M. Edge *et al.*, J. Phys. A: Math. Nucl. Gen., **6**, 1612 (1973);
   M. Nagano *et al.*, J. Phys. G:Nucl. Part. Phys., **10**, 1295 (1984);
   Y. Dai *et al.*, J.Phys.G: Nucl. Part. Phys., **14**, 793 (1998);
   M. Roth *et al.*, Auger collaboration, Proc. 28th ICRC, Tsukuba, Japan, Vol. 2, 333 (2003).
3. A. Haungs *et al.*, KASCADE-Grande collaboration, Proc. 28th ICRC, Tsukuba, Japan, Vol. 2, 985 (2003).
4. H. Rebel and O. Sima *et al.*, KASCADE-Grande collaboration, Proc. 29th ICRC, Pune, India, Vol. 6, 297 (2005);
   I. M. Brancus *et al.*, KASCADE-Grande collaboration, Proc. 29th ICRC, Pune, India, Vol. 6, 361 (2005).
5. O. Sima *et al.*, Report FZKA 6985, Forschungszentrum Karlsruhe, 2004.
6. G. Toma *et al.*, Proc. 26th ECRS, Lisbon, Portugal, so-134, 2006; CERN program library, GEANT user's guide, 1997.
7. J. Linsley *et al.*, Journ. Phys. Soc. Japan, **17**, A-III (1962).